RSC Advances

PAPER

View Article Online
View Journal | View Issue

Cite this: *RSC Adv.*, 2024, **14**, 29559

Interaction mechanism of Al_2O_3 abrasive in tantalum chemical mechanical polishing

Rui Lei,[a] Liang Jiang, *[a] Honglin Zhang,[a] Yushan Chen,[a] Jiaxin Zheng,[a] Junhui Sun, [ab] Qijian Zhao*[c] and Linmao Qian [a]

Received 21st May 2024
Accepted 19th August 2024

DOI: 10.1039/d4ra03743j

rsc.li/rsc-advances

Al_2O_3 abrasive is expected to enhance chemical mechanical polishing (CMP) efficiency compared to the SiO_2 abrasive. However, Al_2O_3 powder has dispersion issues and the material removal mechanism by Al_2O_3 remains unclear. This study investigated the role of Al_2O_3 abrasive in the tantalum CMP. It is revealed that $(NaPO_3)_6$ can effectively disperse Al_2O_3 powder in water. PO_3^- improves the stability while Na^+ deteriorates it. The total Na^+ concentration should be lower than the turning point to attain high stability. With stable Al_2O_3-containing slurries, a relatively high material removal rate of tantalum can be obtained at an alkaline pH. The characterization results indicate that the Ta element can be adsorbed on Al_2O_3 probably due to the chemical interaction between Al_2O_3 and the tantalum surface. Moreover, the Al_2O_3 microsphere tip starts to remove tantalum at 0.48 GPa, which is much lower than the yield strength of the tantalum surface film. For the mechanism, tantalum can be oxidized by H_2O_2 at alkaline pH. When Al_2O_3 presses and slides on the tantalum surface, tribochemical reactions occur, forming a chemical bond of Al–O–Ta at the interface. As Al_2O_3 moves, the bond is stretched and tantalum is detached. The findings provide mechanistic insight into Al_2O_3 abrasive in CMP.

1 Introduction

Tantalum/tantalum nitride has been widely used as the barrier layer for copper interconnect in integrated circuits (IC) because it can prevent copper diffusion and has good adhesion with copper and the dielectric.[1] In the dual-damascene process for fabricating copper interconnect, tantalum/tantalum nitride will be polished in the P3 stage of chemical mechanical polishing (CMP) to achieve local and global planarization, enabling the subsequent photolithography.[2] With the rapid development of IC, it is important to continuously improve the CMP performance of tantalum (tantalum nitride is quite like tantalum in terms of CMP) such as the CMP efficiency.

Tantalum CMP can be considered a nanoscale corrosive wear process, which is mainly affected by the interaction between the tantalum surface and abrasive.[3–5] Therefore, abrasive plays a critical role in the tantalum CMP. At present, SiO_2 is primarily used in the tantalum CMP. Li *et al.*[4,6] used several types of SiO_2 with different specific surfaces to polish tantalum. It was revealed that the tantalum material removal rate (MRR) increases with the specific surface of SiO_2 increasing. This may be because a larger specific surface possesses a higher Si–OH content on the SiO_2 surface, resulting in more intensive chemical interaction between the tantalum surface and SiO_2. Li *et al.*[7] used SiO_2 with different hydroxyl contents to polish tantalum. The experimental results showed that the tantalum MRR is linearly proportional to the hydroxyl content on the SiO_2 surface. In addition, a large amount of tantalum is found on the SiO_2 surface after polishing using atomic absorption spectrophotometry. It was concluded that a strong chemical interaction exists between tantalum and hydroxyl groups on the SiO_2 surface. Vijayakumar *et al.*[8] put forward the polishing mechanism of tantalum by SiO_2. Hydroxyl groups on the SiO_2 surface can react with tantalum to form Si–O–Ta bonds. As SiO_2 moves, the bonds are mechanically torn, leading to the removal of tantalum.

Researchers also used Al_2O_3 as the abrasive in the tantalum CMP. Li *et al.*[6] compared the polishing performance of Al_2O_3 and SiO_2 in the tantalum CMP. The experimental results showed that Al_2O_3 can achieve a higher tantalum MRR than SiO_2. Li *et al.*[7] revealed that not only the hardness of the abrasive and the tantalum surface but also the hydroxyl group on the abrasive surface affects the tantalum removal. When using Al_2O_3 with different bulk densities to polish tantalum, Al_2O_3 with a higher bulk density can attain a higher tantalum MRR. This is because an increased hydroxyl content on Al_2O_3 results in stronger interaction between Al_2O_3 and the tantalum surface.

[a]*Tribology Research Institute, State Key Laboratory of Rail Transit Vehicle System, Southwest Jiaotong University, Chengdu 610031, China. E-mail: jiangliang@swjtu.edu.cn*

[b]*State Key Laboratory of Solid Lubrication, Lanzhou Institute of Chemical Physics, Chinese Academy of Sciences, Lanzhou 730000, China*

[c]*Institute of Machinery Manufacturing Technology, China Academy of Engineering Physics, Mianyang 621900, China. E-mail: zqj@zju.edu.cn*

Compared to the commonly used SiO_2, Al_2O_3 is expected to enhance the CMP efficiency further. However, the interaction mechanism between Al_2O_3 and the tantalum surface has not been investigated in-depth. Moreover, based on our preliminary tests, Al_2O_3 powder has a dispersion issue in water, hindering the development of Al_2O_3-containing slurries. Therefore, this study first used an effective dispersant $(NaPO_3)_6$ to disperse Al_2O_3 powder in ultrapure water. Then, stable Al_2O_3-containing slurries were prepared, and their polishing performance was studied. Afterward, transmission electron microscopy (TEM), energy dispersive spectroscopy (EDS), atomic force microscopy (AFM), and first-principles calculation were performed. Based on the experimental results, the role of Al_2O_3 abrasive in the tantalum CMP was revealed. The findings provide new insights into the material removal mechanism of tantalum in CMP.

2 Experimental details

Al_2O_3 powder (AEROXIDE Alu C, purchased from Evonik Industrial AG) was used as the abrasive. Sodium hexametaphosphate ($(NaPO_3)_6$) was used as the dispersant to disperse Al_2O_3 powder in ultrapure water, preparing an Al_2O_3 suspension.[9] Specifically, $(NaPO_3)_6$ was first dissolved in ultrapure water. Then, Al_2O_3 powder was added under continuous stirring. Afterwards, the Al_2O_3 suspension was stirred for 1 h and sonicated for 15 min. Finally, if necessary, $NaNO_3$ was added to the Al_2O_3 suspension to provide Na^+ and control the total Na^+ concentration. To characterize the long-term stability of the Al_2O_3 suspension, it was allowed to stand for 24 h, and then the turbidity values of the upper layer and the bottom layer of the suspension were measured with a turbidity meter (WZS-188, Shanghai Yidian Scientific Instrument Co., Ltd.). After obtaining a relatively stable Al_2O_3 suspension, tantalum CMP slurries were prepared by adding additional H_2O_2 and adjusting pH (dilute NaOH and HNO_3). All the above chemical reagents were purchased from Sinopharm Chemical Reagent Co., Ltd.

In the CMP experiments, a tantalum disk (50.8 mm diameter, 99.99% purity, China New Metal Materials Technology Co., Ltd.) was polished on a benchtop polisher (UNIPOL-1200S, Shenyang Kejing Auto-Instrument Co., Ltd.). Table 1 shows the CMP process conditions. During polishing, the CMP slurry was stirred continuously to maintain excellent dispersion. The weights of the tantalum disk before and after polishing were measured with a microbalance (0.01 mg readability, MSA225S, Sartorius). The MRR was calculated with the weight loss method.[10] In particular, the density of tantalum is 16.68 g cm^{-3}.[11] The topographies and surface roughness S_a of the tantalum disk after polishing were measured with an optical surface profiler (SuperView W1, Chotest). The scan area was 97.9 μm × 97.9 μm. Each CMP slurry was repeated four times.

To explore the interaction between Al_2O_3 and tantalum, the CMP slurry was used 1 time, 10 times repeatedly and 20 times repeatedly, and then collected after polishing. The topography and compositional distribution of Al_2O_3 abrasive in the recycled slurry were characterized with TEM (Talos F200X, FEI) and EDS.

In order to investigate the interaction between Al_2O_3 and tantalum surface further, the adhesion force between an Al_2O_3 microsphere tip (2.5 μm nominal radius. The AFM probe was purchased from Novascan Technologies, Inc. It had a spring constant of 14.08 N m^{-1} calibrated by the thermal noise method[12]) and the tantalum surface was measured in the designated solution on an atomic force microscope (MFP-3D, Asylum Research). The dwell time was varied. The experimental conditions were as follows: 1 μm distance, 500 nm s^{-1} velocity, 0.5 μN applied load, and 0 s/5 s/10 s dwell time.

Moreover, AFM wear experiments were carried out to simulate the tantalum material removal process by the Al_2O_3 abrasive in CMP on another atomic force microscope (E-sweep, Hitachi). An Al_2O_3 microsphere tip was rubbed against the tantalum surface in the designated solution. The applied load was varied. The experimental conditions were as follows: 0.1 μN/0.2 μN/0.4 μN/0.6 μN/0.8 μN applied load, 1 μm s^{-1} relative sliding velocity, 2 μm relative sliding distance, and 100 reciprocating sliding cycles. After the AFM wear experiments, the topographies of the wear areas on the tantalum surface were scanned with a Si_3N_4 probe (MSCT, Bruker) in a vacuum. Moreover, the profile of the Al_2O_3 microsphere tip was measured by scanning a grating sample (TGT1, NT-MDT). The scanning result exhibits a reverse image of the Al_2O_3 microsphere tip rather than that of the grating sample because the curvature of the microsphere tip is much larger than that of the grating spikes.

To prepare a relatively smooth tantalum surface for the above AFM experiments regarding the adhesion force and wear, a small tantalum sample (10 mm × 10 mm, cut from a complete wafer purchased from SKW, Associates, Inc.) was pre-polished, then cleaned with ultrapure water and dried. The CMP slurry contained ultrapure water, 2 wt% colloidal SiO_2 (YZ8040, purchased from Shanghai YZ-Lapping Material Co., Ltd.), 0.2 wt% H_2O_2, and at pH 10. Fig. 1 shows the topography and the average cross-sectional profile along the A–B direction.

Table 1 CMP process conditions in this study

Condition	Value
Down force	5.0 kg set pressure displayed on the panel
Carrier speed	60 rpm
Platen speed	60 rpm
Slurry flow rate	100 mL min^{-1}
Time of each polishing	1 min
Polishing pad	Politex (Dow, conditioned for 30 s with a brush before each polishing)

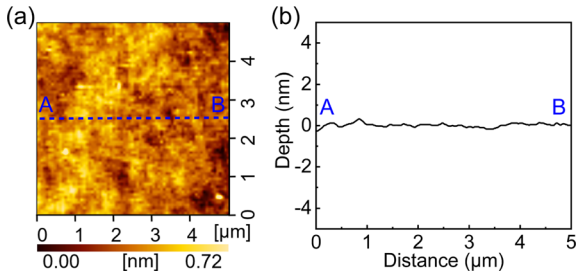

Fig. 1 AFM measurement results of the tantalum wafer surface after polishing. (a) The topography. (b) The average cross-sectional profile along the A–B direction.

As can be seen, after polishing, the tantalum wafer surface is very smooth, meeting the requirement of AFM experiments.

To confirm the interaction between Al_2O_3 and tantalum, first-principles calculation based on density functional theory (DFT) was conducted using the Cambridge Sequential Total Energy Package. The exchange-correlation function was described using the generalized gradient approximation of Perdew–Burke–Ernzerhof.[13] The projector-augmented wave potential was used in depicting interactions formed between electrons and ions. The Brillouin zone was sampled using Monkhorst–Pack 8 × 8 × 1 *k*-point grids. The calculation parameters for the plane-wave cutoff energy, total energy, and convergence tolerance force were set as 450 eV, 1×10^{-6} eV, and 0.02 eV $Å^{-1}$ for accurate calculations. The spin interactions were considered, and a 15 Å vacuum layer was used to prevent periodic interactions.

3 Results and discussion

3.1 Stability of Al_2O_3 suspensions

Stability is a significant indicator of the CMP slurry. Unstable CMP slurry may result in severe defects such as scratches on the workpiece surface after polishing.[14] To this end, this study used $(NaPO_3)_6$ to disperse Al_2O_3 powder in ultrapure water. Generally, cations, such as Na^+, will be introduced to the tantalum CMP slurry unavoidably, for example during adjusting the pH value. Based on the existing research, PO_3^- of $(NaPO_3)_6$ can improve the stability of Al_2O_3, whereas Na^+ and other cations may deteriorate it.[15] To explore the stability boundaries of Al_2O_3 suspensions under different concentrations of PO_3^-, different amounts of Na^+ (mainly from $NaNO_3$) were added on purpose. After standing for 24 h, the stability of the Al_2O_3 suspension was characterized by measuring the turbidity values of the bottom layer and upper layer of the suspension. If the difference between the two turbidity values (denoted as ΔTurbidity) fluctuates within a small range of 100–400 NTU and no apparent precipitate appears on the bottom, it suggests that the Al_2O_3 suspension is relatively stable; otherwise, it is unstable.

Fig. 2 shows the stability results of the Al_2O_3 suspensions. As shown in Fig. 2(a), as the total Na^+ concentration increases,

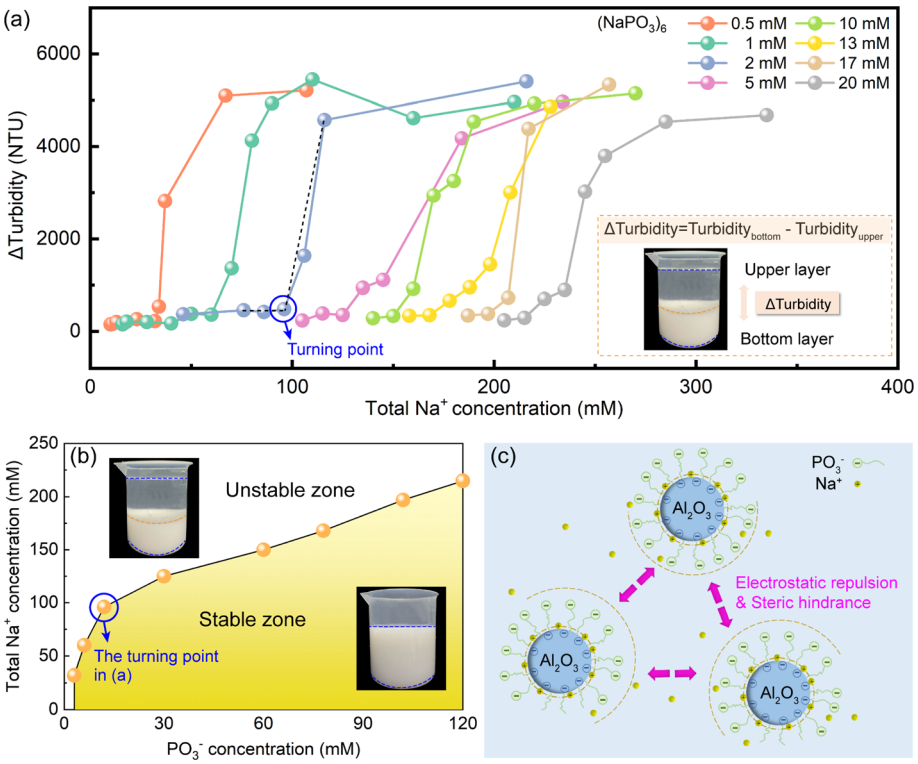

Fig. 2 Stability results of the Al_2O_3 suspensions. (a) The effect of the total Na^+ concentration on the stability of the Al_2O_3 suspension. In the experiments, $(NaPO_3)_6$ concentrations were set as 0.5 mM, 1 mM, 2 mM, 5 mM, 10 mM, 13 mM, 17 mM, and 20 mM. The abscissa is the total Na^+ concentration in the Al_2O_3 suspension, and the ordinate is ΔTurbidity after letting the Al_2O_3 suspension stand for 24 h. (b) The turning points of the total Na^+ concentration corresponding to different PO_3^- concentrations. (c) The dispersion mechanism of Al_2O_3 by $(NaPO_3)_6$.

ΔTurbidity first remains at about 100–400 NTU, then it reaches a turning point and then sharply increases until it gradually saturates. When the total Na^+ concentration exceeds the turning point, the Al_2O_3 suspension becomes unstable, and an apparent precipitate appears on the bottom of the beaker. Fig. 2(b) summarizes the turning points of the total Na^+ concentration corresponding to different concentrations of PO_3^-. As can be seen, the upper left unstable and bottom right stable zones are separated by the turning points. Moreover, as the PO_3^- concentration increases, the turning point of the total Na^+ concentration gradually increases.

Fig. 2(c) shows the effects of PO_3^- and Na^+ on the dispersion of Al_2O_3. For the mechanism, $(NaPO_3)_6$ can be hydrolyzed in an aqueous solution to form long chain structures in which there are a lot of negatively charged PO_3^-.[16] PO_3^- can be adsorbed on the Al_2O_3 surface probably through hydrogen bonding.[17,18] On the one hand, the zeta potential of Al_2O_3 becomes more negative due to the adsorbed negatively charged PO_3^-. On the other hand, the steric hindrance between Al_2O_3 increases due to the long-chain structure of the adsorption layer.[16] Therefore, the stability of Al_2O_3 is improved. As for Na^+, it can enter the electric double layer of Al_2O_3, neutralizing the zeta potential and compressing the electric double layer. Consequently, the stability of Al_2O_3 is weakened.

In summary, PO_3^- and Na^+ play opposite roles in dispersing Al_2O_3. For a certain concentration of PO_3^-, the total Na^+ concentration should be lower than the turning point to attain high stability when preparing an Al_2O_3-containing slurry.

3.2 CMP performance of Al_2O_3-containing slurries

Based on the above stability results, 5 mM $(NaPO_3)_6$ was chosen to disperse 1 wt% Al_2O_3 powder in ultrapure water to prepare an Al_2O_3 suspension. Fig. 3(a) shows the stability results. After standing for 24 h, the Al_2O_3 suspension at the natural pH value is quite stable without any apparent precipitate on the bottom of the beaker. The average particle size is 142 nm.

On this basis, a tantalum CMP slurry containing ultrapure water, 1 wt% Al_2O_3 powder, 5 mM $(NaPO_3)_6$, 0.4 wt% H_2O_2 and 10 mM NaOH was prepared. The stability was examined at different pH values. Fig. 3(b) shows the stability results. After standing for 24 h, the Al_2O_3-containing slurries at pH 2 to 10 are all very stable and can be used for the following CMP.

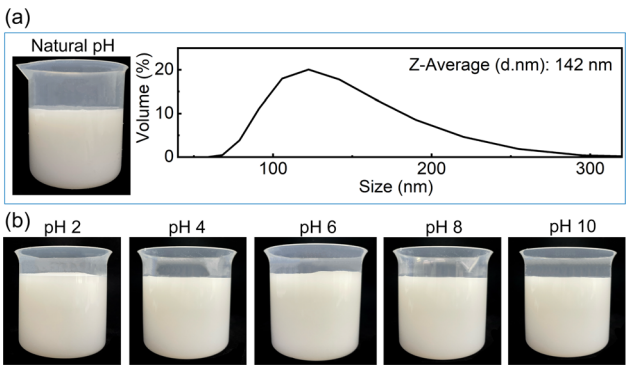

Fig. 3 Stability results of the Al_2O_3 suspension and slurries with 5 mM $(NaPO_3)_6$ as the dispersant. (a) The Al_2O_3 suspension at the natural pH after standing for 24 h. The particle size distribution was measured by Zetasizer Nano (Malvern Instruments Ltd.). (b) The Al_2O_3-containing slurries at pH 2 to 10 after standing for 24 h.

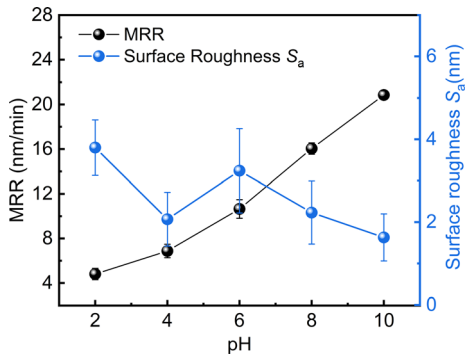

Fig. 4 MRR and surface roughness S_a results after polishing with the Al_2O_3-containing slurries at different pH values.

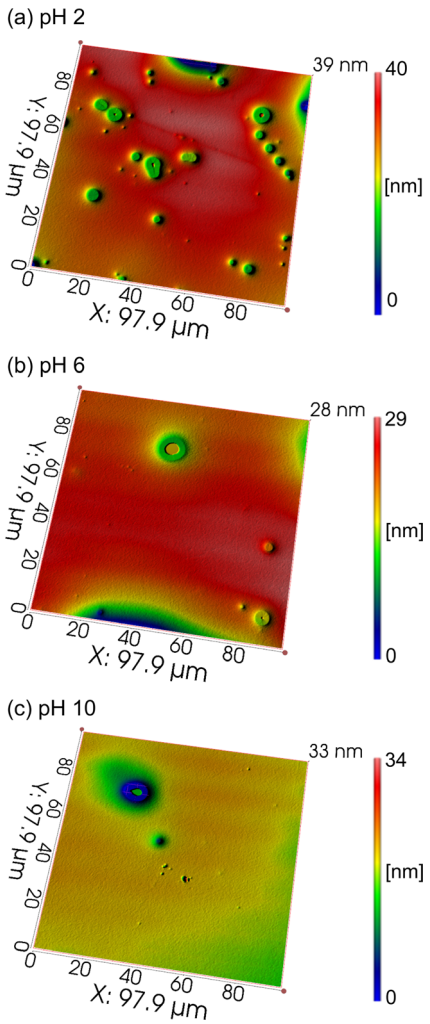

Fig. 5 Corresponding topographies of tantalum after polishing with the Al_2O_3-containing slurries at different pH values. (a) pH 2. (b) pH 6. (c) pH 10.

Fig. 4 shows the MRR and surface roughness S_a results of tantalum after polishing with the above stable slurries at different pH values. With the increase in the pH value, the MRR gradually increases. The MRR reaches the maximum value at pH 10. Overall, the surface roughness S_a first decreases and then tends to be stable. The surface roughness S_a reaches 1.6 nm at pH 10.

Fig. 5 shows the corresponding topographies of tantalum after polishing. At pH 2, the topography is quite rough with many surface defects. In comparison, at pH 10, the topography becomes much smoother, and the surface defects are largely reduced.

To conclude, at pH 10, a relatively high MRR and satisfactory surface quality of tantalum can be obtained. Therefore, alkaline pH is recommended for the Al_2O_3-containing CMP slurry for tantalum.

3.3 TEM and EDS characterization of Al_2O_3 before and after CMP

The above results reveal that Al_2O_3 can be used as an effective abrasive for the tantalum CMP. To explore the role of Al_2O_3 in the tantalum CMP, we used TEM and EDS to characterize Al_2O_3 before and after polishing, aiming to investigate the interaction between Al_2O_3 and the tantalum surface. Fig. 6 shows the TEM dark-field images and EDS results. As shown in Fig. 6(a), before polishing, Al_2O_3 in the slurry contains Al, O, P and Na elements. Al is from Al_2O_3, O can be from Al_2O_3 and $(NaPO_3)_6$, P is from $(NaPO_3)_6$, while Na can be from $(NaPO_3)_6$ and NaOH. As shown

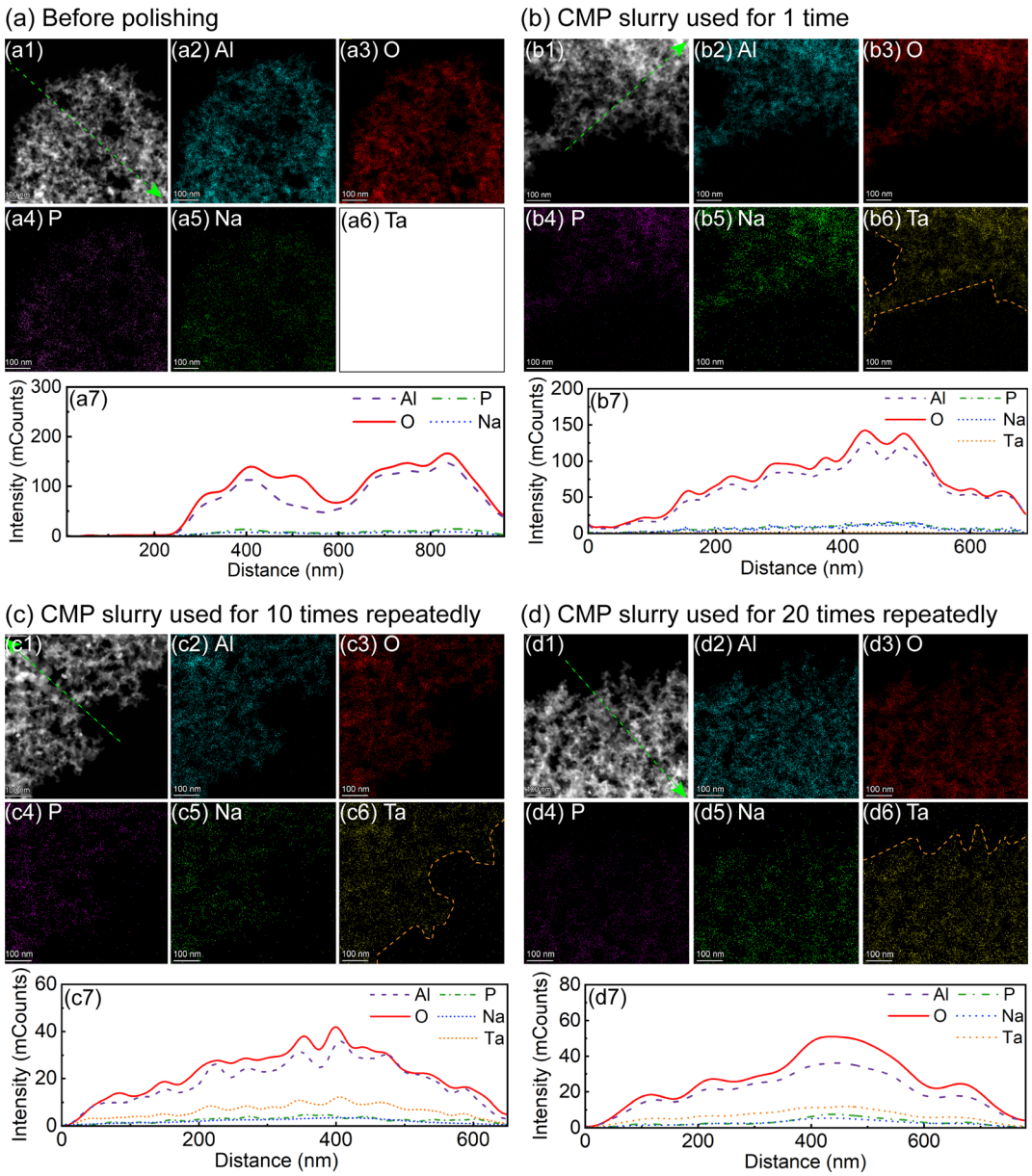

Fig. 6 TEM dark-field images and EDS results of Al_2O_3 in the used slurries. (a) Before polishing. (b) After polishing with the CMP slurry used for 1 time. (c) After polishing with the CMP slurry used for 10 times repeatedly. (d) After polishing with the CMP slurry used for 20 times repeatedly.

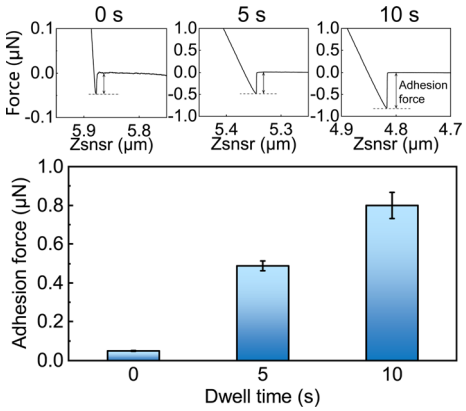

Fig. 7 The force–distance curves and the corresponding statistics of the adhesion force between the Al_2O_3 microsphere tip and the tantalum surface in the solution containing ultrapure water, 0.4 wt% H_2O_2, 5 mM Na^+, and at pH 10. The applied load was fixed at 0.5 μN. The dwell time was varied.

in Fig. 6(b) to (d), after polishing with the same CMP slurries 1 time, 10 times repeatedly, and 20 times repeatedly, the Ta element can be observed, and the distribution areas almost coincide with those of Al, O, P and Na. This suggests that Ta element can be adsorbed on the active sites of the Al_2O_3 surface, which may be the reason for the excellent CMP performance of the Al_2O_3-containing slurry at pH 10. In addition, the active sites may include hydroxyl group sites, Al^{3+} sites, and so on.[19,20]

3.4 AFM characterization of the interaction between Al_2O_3 and tantalum

The above TEM and EDS results indicate that Ta can be adsorbed on the Al_2O_3 surface. We used AFM to explore the adsorption from the microscopic perspective. The adhesion force between the Al_2O_3 microsphere tip and the tantalum surface in the solution was measured. The solution contained ultrapure water, 0.4 wt% H_2O_2, 5 mM Na^+, and at pH 10. Fig. 7 shows the variation trend of the adhesion force with the dwell time. Under an applied load of 0.5 μN, the adhesion force gradually increases from 0.048 to 0.799 μN as the dwell time increases from 0 to 10 s. In principle, the adhesion force can be affected by van der Waals force, electrostatic force, capillary force, and chemical interaction.[21,22] The capillary force can be neglected in the CMP slurry.[23,24] Under the fixed applied load, the van der Waals force and electrostatic force remain basically unchanged, suggesting that the increased adhesion force is mainly attributed to the enhanced chemical interaction. Additionally, according to the research of Li *et al.*[25] and Tian *et al.*,[26] the increased dwell time will lead to an increase in the number of chemical bonds formed, resulting in an enhancement of the interfacial interaction. Therefore, it can be concluded that

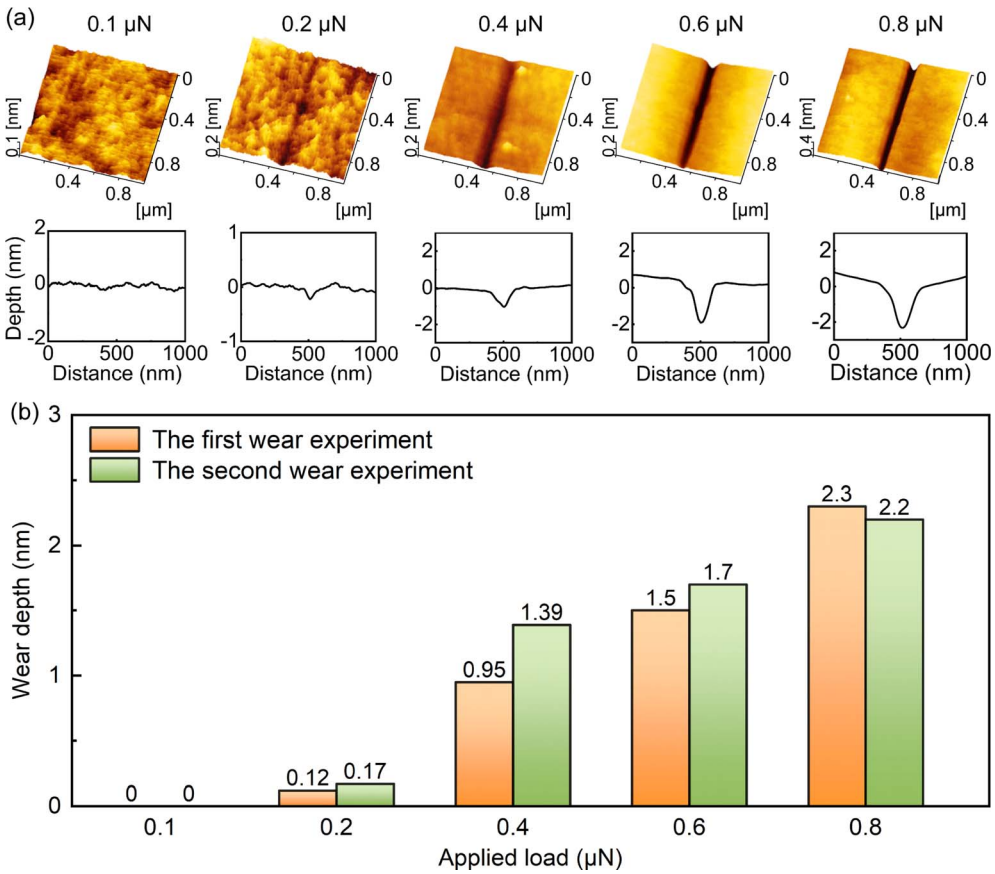

Fig. 8 Results of the AFM wear experiments under different applied loads in the solution containing ultrapure water, 0.4 wt% H_2O_2, 5 mM Na^+, and pH 10. (a) The topographies and average cross-section profiles of the wear areas. (b) The statistical results of the wear depth.

chemical interaction can exist between Al_2O_3 and the tantalum surface, which can affect the material removal in the tantalum CMP. In the following study, we performed first-principles calculation to investigate the chemical interaction between Al_2O_3 and the tantalum surface.

AFM wear experiments were performed to examine whether the chemical interaction between Al_2O_3 and the tantalum surface can affect the material removal of tantalum. An Al_2O_3 microsphere tip was rubbed against the tantalum surface in the solution, simulating the tantalum CMP. The solution contained ultrapure water, 0.4 wt% H_2O_2, 5 mM Na^+, and at pH 10. Fig. 8 shows the AFM wear results of tantalum. In particular, each condition was repeated twice to avoid excessive wear of the Al_2O_3 microsphere tip, similar to the literature.[27–29] As shown in Fig. 8(a), no wear scar can be observed on the tantalum surface at 0.1 μN applied load. In comparison, a shallow wear scar appears on the tantalum surface at 0.2 μN. Moreover, as the applied load increases from 0.2 μN to 0.8 μN, the wear scar becomes deeper and clearer, and the wear depth gradually increases from about 0.1 nm to 2.3 nm (as shown in Fig. 8(b)).

Fig. 9 exhibits the Al_2O_3 microsphere tip after the wear experiments. No apparent wear track can be observed on the Al_2O_3 tip, and the profile is still spherical. The fitting radius of the Al_2O_3 tip is about 3.116 μm, which is close to the nominal value. In our case, Hertz contact theory was used to roughly estimate the contact pressure between the Al_2O_3 tip and the tantalum surface. At 0.2 μN applied load, the maximum contact pressure is calculated to be 0.48 GPa ($P_{max} = (6F_{applied}E^{*2}/\pi^3R^2)^{1/3}$. For calculation, $F_{applied}$ is the applied load, that is 0.2 μN here; $E^* = [(1 - \nu_1^2)/E_1 + (1 - \nu_2^2)E_2]^{-1}$.[30] The Young's modulus E_1 and Poisson ratio ν_1 of tantalum are 186 GPa and 0.35, respectively.[31] The Young's modulus E_2 and Poisson ratio ν_2 of Al_2O_3 are 370 GPa and 0.22, respectively;[32] R is the radius of the Al_2O_3 microsphere tip).

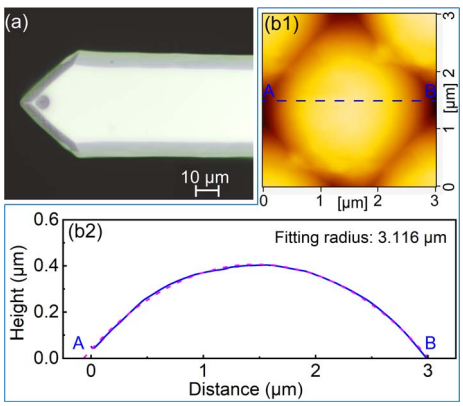

Fig. 9 Al_2O_3 microsphere tip after the AFM wear experiments. (a) The optical image of the Al_2O_3 tip. It was measured with an optical microscope (Axio Lab.A1, ZEISS). (b1) The AFM inverse image of the Al_2O_3 tip. (b2) The cross-sectional profile of the Al_2O_3 tip along A–B in (b1). The dashed line in (b2) is the fitting curve.

Generally, yield strength is positively correlated with hardness.[33] As reported by Hariharaputhiran *et al.*,[34] the bulk hardness of the tantalum surface film is 1100–1200 kg mm^{-2}, which is much larger than 230 kg mm^{-2} of tantalum. Therefore, it can be inferred that the yield strength of the tantalum surface film should be higher than that of tantalum. As shown in Fig. 8(a), a shallow wear scar appears on the tantalum surface at 0.2 μN. Combined with the calculation result based on Hertz contact theory, the material removal of tantalum starts at a contact pressure of 0.48 GPa, which is much lower than the yield strength of tantalum (about 6–19 GPa (ref. 35 and 36)), let alone that of the tantalum surface film.

To conclude, Al_2O_3 can remove tantalum in the slurry under a contact pressure much lower than the yield strength of the tantalum surface film, which is quite similar to the material removal of silicon.[37] A reasonable explanation can be that when Al_2O_3 slides on the tantalum surface, tribochemical reactions occur, lowering the energy barrier for dissociation of the interfacial bond and/or the subsurface back bond.[38]

3.5 First-principles calculation of interaction between Al_2O_3 and tantalum

In this section, we performed first-principles calculations based on DFT to further explore the interaction between Al_2O_3 and the tantalum surface. As reported, tantalum can be oxidized to Ta_2O_5 in the H_2O_2-containing slurry at alkaline pH.[5,39] Therefore, the interaction between Al_2O_3 and Ta_2O_5 was investigated. Fig. 10(a) exhibits the models of Al_2O_3, Ta_2O_5 and the Al_2O_3/

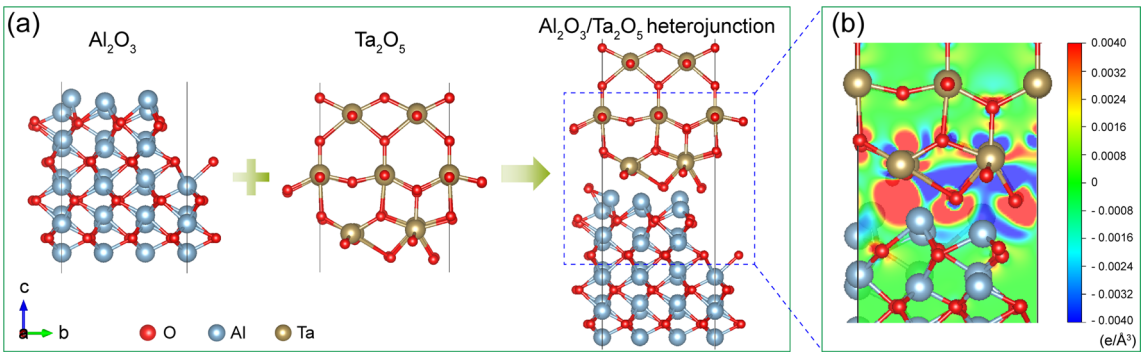

Fig. 10 Establishment of the Al_2O_3/Ta_2O_5 heterojunction model and calculation of the charge density difference. (a) The Al_2O_3/Ta_2O_5 heterojunction model. (b) The charge density difference of the Al_2O_3/Ta_2O_5 heterojunction at the interface.

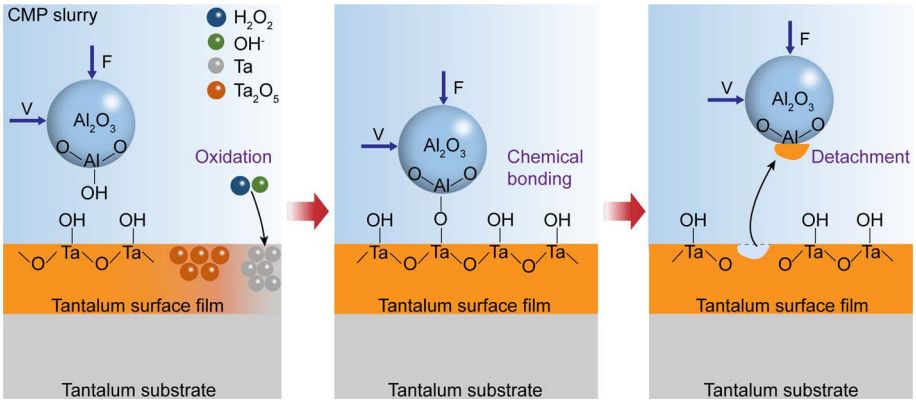

Fig. 11 Schematic diagram of the role of Al_2O_3 abrasive in the tantalum CMP.

Ta_2O_5 heterojunction. The binding energy of the Al_2O_3/Ta_2O_5 heterojunction can be calculated as follows:

$$E = E_{Al_2O_3} + E_{Ta_2O_5} - E_{Al_2O_3/Ta_2O_5} \quad (1)$$

$E_{Al_2O_3}$, $E_{Ta_2O_5}$, $E_{Al_2O_3/Ta_2O_5}$ are the energies of Al_2O_3, Ta_2O_5, and the Al_2O_3/Ta_2O_5 heterojunction, which are calculated to be −438.52 eV, −400.92 eV, and −863.46 eV, respectively.[40] By simple calculation, the binding energy of the Al_2O_3/Ta_2O_5 heterojunction is 24.02 eV, indicating a strong interaction existing between Al_2O_3 and Ta_2O_5.[41]

Moreover, the charge density difference of the Al_2O_3/Ta_2O_5 heterojunction is obtained by subtracting the isolated bottom (Al_2O_3) and upper (Ta_2O_5) surfaces from the total interface (the Al_2O_3/Ta_2O_5 heterojunction). As shown in Fig. 10(b), the red and blue areas indicate enrichment and depletion of the electron due to the interaction between Al_2O_3 and Ta_2O_5, respectively. The Al_2O_3 side is surrounded by red areas, while the Ta_2O_5 side is surrounded by blue areas, suggesting that electrons transfer from Ta_2O_5 to Al_2O_3, and form a chemical bond of Al–O–Ta at the Al_2O_3/Ta_2O_5 interface, which may weaken the Ta–O back bond and facilitate the removal of Ta atoms to some extent.[42]

3.6 Role of Al_2O_3 abrasive in tantalum CMP

Based on the results obtained so far and the literature, the role of Al_2O_3 abrasive in the tantalum CMP can be proposed. Fig. 11 demonstrates the corresponding schematic diagram. In the H_2O_2-containing slurry at alkaline pH, tantalum can be oxidized to form an oxide layer on the surface, which is mainly composed of Ta_2O_5 and Ta–OH complexes with hydroxyl groups. The chemical reactions can be depicted as follows:[39,43]

$$6Ta + 10H_2O_2 + 10OH^- \rightarrow 3Ta_2O_5 + 15H_2O + 10e^- \quad (2)$$

$$Ta^{5+} + x/2H_2O_2 + xe^- \rightarrow Ta(OH)_x^{(5-x)+} \quad (3)$$

$$Ta^{5+} + (x/2 + 1)H_2O_2 + (x + 2)e^- \rightarrow TaO(OH)_x^{(3-x)+} + H_2O \quad (4)$$

Moreover, Al_2O_3 can also be hydrolyzed to form hydroxyl groups.[7]

When Al_2O_3 presses and slides on the tantalum surface, similar to silicon,[38,44] tribochemical reactions can occur. Hydroxyl groups on the two contact surfaces are close to each other, and a dehydration reaction may occur to form the chemical bond of Al–O–Ta at the interface (partly confirmed by the above first-principles calculation).[45,46] As Al_2O_3 moves, the interfacial chemical bond is stretched, and tantalum is detached from the tantalum surface. Eventually, the material removal of tantalum is achieved. In particular, as revealed by the AFM wear experimental results, the threshold contact pressure is much lower than the yield strength of the tantalum surface film when tantalum is removed, implying that the formation and stretching of the chemical bond of Al–O–Ta may lower the energy barrier for the dissociation of the Ta–Ta bond and/or Ta–O bond (weakening of the Ta–O back bond is confirmed by the above first-principles calculation).[37]

In addition, Li *et al.*[6] and Hariharaputhiran *et al.*[34] used Al_2O_3 (the mean aggregate size is 290–360 nm, Ferro Electronics) to polish tantalum. The MRR decreases with the increase in the hardness of the softening layer on the tantalum surface. Therefore, it can be concluded that Al_2O_3 may have a mechanical effect. Likewise, Al_2O_3 in this study may also mechanically abrade the tantalum surface besides chemical bonding. More investigation is ongoing.

This study suggests that chemical interaction exists between Al_2O_3 and the tantalum surface, helping achieve the material removal of tantalum. Therefore, to further enhance the CMP efficiency of tantalum, it is recommended to continuously increase the active sites that bind tantalum on the Al_2O_3 surface, for example hydroxyl groups.[47]

4 Conclusions

This study investigated the interaction mechanism of Al_2O_3 abrasive in the tantalum CMP using CMP and several characterization techniques including TEM, EDS, AFM, and first-principles calculation. Based on the results obtained so far, the conclusions can be drawn as follows:

(1) $(NaPO_3)_6$ can be used as an effective dispersant for Al_2O_3 powder in water. PO_3^- can improve the stability of Al_2O_3 through electrostatic repulsion and steric hindrance, while Na^+ deteriorates it. The total Na^+ concentration should be lower than the turning point to attain a highly stable Al_2O_3

suspension. For the tantalum CMP, with stable Al_2O_3-containing slurries, a relatively high MRR and satisfactory surface quality of tantalum can be obtained at pH 10.

(2) TEM and EDS characterization results indicate that Ta element can be absorbed on the Al_2O_3 surface, which can be attributed to the chemical interaction between Al_2O_3 and the tantalum surface (confirmed by AFM adhesion force measurement), forming the chemical bond of Al–O–Ta (partly confirmed by first-principles calculation). Moreover, AFM wear experimental results show that the Al_2O_3 microsphere tip can remove tantalum under 0.48 GPa, which is much lower than the yield strength of the tantalum surface film.

(3) For the CMP mechanism, with H_2O_2 and at alkaline pH, tantalum can be oxidized to Ta_2O_5 and Ta–OH complexes, and Al_2O_3 can be hydrolyzed. When Al_2O_3 presses and slides on the tantalum surface, tribochemical reactions can occur. Hydroxyl groups on the two contact surfaces may be dehydrated to form the chemical bond of Al–O–Ta at the interface. As Al_2O_3 moves, the interfacial chemical bond is stretched, and tantalum is detached. Eventually, the material removal of tantalum is achieved.

Data availability

The data that support the findings of this study are available from the corresponding author upon reasonable request.

Conflicts of interest

There are no conflicts of interest to declare.

Acknowledgements

This work is supported by the National Natural Science Foundation of China (51991373, and 52235004), the National Key R&D Program of China (2020YFA0711001), and the Fundamental Research Funds for the Central Universities (2682024CG007).

References

1 M. Lane, R. H. Dauskardt, N. Krishna and I. Hashim, *J. Mater. Res.*, 2000, **15**, 203–211.
2 Y. Li, *Microelectronic Applications of Chemical Mechanical Planarization*, John Wiley & Sons, Inc., Hoboken, New Jersey, USA, 2007.
3 S. V. Babu, A. Jindal and Y. Li, *JOM*, 2001, **53**, 50–52.
4 Y. Li, M. Hariharaputhiran and S. V. Babu, *J. Mater. Res.*, 2001, **16**, 1066–1073.
5 J. Zhang, S. Li and P. W. Carter, *J. Electrochem. Soc.*, 2007, **154**, H109.
6 Y. Li, S. Ramarajan, M. Hariharaputhiran, Y. S. Her and S. V. Babu, *MRS Proc.*, 2000, **613**, E2.4.1.
7 Y. Li, J. Zhao, P. Wu, Y. Lin, S. V. Babu and Y. Li, *Thin Solid Films*, 2006, **497**, 321–328.
8 A. Vijayakumar, T. Du, K. B. Sundaram and V. Desai, *Microelectron. Eng.*, 2003, **70**, 93–101.
9 M. Kitayama and J. A. Pask, *J. Am. Ceram. Soc.*, 1996, **79**, 2003–2011.
10 G. Xiao, L. Jiang, W. Peng, J. Liu, C. Deng and L. Qian, *Wear*, 2022, **508–509**, 204466.
11 H. Yang, J. Li, Z. Zhou and J. Ruan, *Mater. Lett.*, 2013, **100**, 152–155.
12 M. L. B. Palacio and B. Bhushan, *Crit. Rev. Solid State Mater. Sci.*, 2010, **35**, 73–104.
13 J. P. Perdew, K. Burke and M. Ernzerhof, *Phys. Rev. Lett.*, 1996, **77**, 3865.
14 A. J. Khanna, S. Gupta, P. Kumar, F.-C. Chang and R. K. Singh, *ECS J. Solid State Sci. Technol.*, 2018, **7**, P423.
15 C. O. Metin, L. W. Lake, C. R. Miranda and Q. P. Nguyen, *J. Nanopart. Res.*, 2011, **13**, 839–850.
16 H. Song, Z. Cao, W. Xie, F. Cheng, K. A. M. Gasem and M. Fan, *J. Cleaner Prod.*, 2019, **235**, 259–271.
17 L. Piani and A. Papo, *J. Eng.*, 2013, **2013**, 930832.
18 Z.-h. Li, Y.-x. Han, Y.-j. Li and P. Gao, *Trans. Nonferrous Met. Soc. China*, 2017, **27**, 1841–1848.
19 H. Knözinger and P. Ratnasamy, *Catal. Rev.*, 1978, **17**, 31–70.
20 N. Tang, Y. Cong, Q. Shang, C. Wu, G. Xu and X. Wang, *ACS Catal.*, 2017, **7**, 5987–5991.
21 M. Binggeli and C. M. Mate, *Appl. Phys. Lett.*, 1994, **65**, 415–417.
22 X. Xiao and L. Qian, *Langmuir*, 2000, **16**, 8153–8158.
23 Q. Ouyang, K. Ishida and K. Okada, *Appl. Surf. Sci.*, 2001, **169–170**, 644–648.
24 P. Liu, S. Hong, S. Jeon, J. Lee, D. Kwak, Y. Wada, H. Hiyama, S. Hamada and T. Kim, *Colloids Surf., A*, 2021, **627**, 127156.
25 Q. Li, T. E. Tullis, D. Goldsby and R. W. Carpick, *Nature*, 2011, **480**, 233–236.
26 K. Tian, N. N. Gosvami, D. L. Goldsby, Y. Liu, I. Szlufarska and R. W. Carpick, *Phys. Rev. Lett.*, 2017, **118**, 076103.
27 A. A. Tseng, *Appl. Surf. Sci.*, 2010, **256**, 4246–4252.
28 F. Ilie, *Tribol.-Mater., Surf. Interfaces*, 2013, **7**, 211–215.
29 K.-H. Chung, Y.-H. Lee, H.-J. Kim and D.-E. Kim, *Tribol. Lett.*, 2013, **52**, 315–325.
30 T. D. B. Jacobs, C. Mathew Mate, K. T. Turner and R. W. Carpick, in *Scanning Probe Microscopy in Industrial Applications*, 2013, pp. 15–48, DOI: **10.1002/9781118723111.ch2**.
31 A. Dorogoy and D. Rittel, *Mech. Mater.*, 2017, **112**, 143–153.
32 T.-H. Fang, T. Wang, C.-H. Liu, L.-W. Ji and S.-H. Kang, *Nanoscale Res. Lett.*, 2007, **2**, 410.
33 E. J. Pavlina and C. J. Van Tyne, *J. Mater. Eng. Perform.*, 2008, **17**, 888–893.
34 M. Hariharaputhiran, Y. Li, S. Ramarajan and S. Babu, *Electrochem. Solid-State Lett.*, 2000, **3**, 95–98.
35 M. Zhang, B. Yang, J. Chu and T. G. Nieh, *Scr. Mater.*, 2006, **54**, 1227–1230.
36 T. P. Remington, C. J. Ruestes, E. M. Bringa, B. A. Remington, C. H. Lu, B. Kad and M. A. Meyers, *Acta Mater.*, 2014, **78**, 378–393.
37 L. Chen, J. Wen, P. Zhang, B. Yu, C. Chen, T. Ma, X. Lu, S. H. Kim and L. Qian, *Nat. Commun.*, 2018, **9**, 1542.
38 L. Chen, H. He, X. Wang, S. H. Kim and L. Qian, *Langmuir*, 2015, **31**, 149–156.

39 T. Du, D. Tamboli, V. Desai, V. S. Chathapuram and K. B. Sundaram, *J. Mater. Sci.: Mater. Electron.*, 2004, **15**, 87–90.
40 L. Huang and X. Zhou, *J. Phys.: Conf. Ser.*, 2023, **2639**, 012013.
41 Y. Liu, G.-J. Zhao, J.-X. Zhang, F.-Q. Bai and H.-X. Zhang, *Appl. Surf. Sci.*, 2021, **549**, 149309.
42 S. FliszÁR and C. Minichino, *J. Phys. Colloq.*, 1987, **48**, 367–375.
43 S. C. Kuiry, S. Seal, W. Fei, J. Ramsdell, V. H. Desai, Y. Li, S. V. Babu and B. Wood, *J. Electrochem. Soc.*, 2003, **150**, C36–C43.
44 C. Chen, C. Xiao, X. Wang, P. Zhang, L. Chen, Y. Qi and L. Qian, *Appl. Surf. Sci.*, 2016, **390**, 696–702.
45 J. Yu, S. H. Kim, B. Yu, L. Qian and Z. Zhou, *ACS Appl. Mater. Interfaces*, 2012, **4**, 1585–1593.
46 Y. Li, X. Sha, W. Yue, W. Qin and C. Wang, *Int. J. Refract. Met. Hard Mater.*, 2019, **79**, 197–203.
47 V. M. Gun'ko, V. V. Turov, V. I. Zarko, E. F. Voronin, V. A. Tischenko, V. V. Dudnik, E. M. Pakhlov and A. A. Chuiko, *Langmuir*, 1997, **13**, 1529–1544.